Distinct Frontal Ablation Processes Drive Heterogeneous Submarine Terminus Morphology

M. J. Fried[1,2] (ID), **D. Carroll**[3,4] (ID), **G. A. Catania**[2,5] (ID), **D. A. Sutherland**[6] (ID), **L. A. Stearns**[7] (ID), **E. L. Shroyer**[8] (ID), and **J. D. Nash**[8] (ID)

[1]ICF, Washington, DC, USA, [2]Institute for Geophysics, University of Texas at Austin, Austin, TX, USA, [3]Moss Landing Marine Laboratories, San José State University, San Jose, CA, USA, [4]Jet Propulsion Laboratory, California Institute of Technology, Pasadena, CA, USA, [5]Department of Geology, University of Texas at Austin, Austin, TX, USA, [6]Department of Earth Sciences, University of Oregon, Eugene, OR, USA, [7]Department of Geology, University of Kansas, Lawrence, KS, USA, [8]College of Earth, Ocean, and Atmospheric Sciences, Oregon State University, Corvallis, OR, USA

Abstract Calving and submarine melt drive frontal ablation and sculpt the ice face of marine-terminating glaciers. However, there are sparse observations of submarine termini, which limit estimates of spatially varying submarine melt. Here we present a detailed survey of a west Greenland glacier to reveal heterogeneity in submarine terminus morphology. We find that the majority of the terminus (~77%) is undercut, driven by calving in the upper water column and submarine melting at depth. The remaining ~23% of the terminus is overcut, driven by calving alone. We use observations of six subglacial discharge outlets, combined with a plume model, to estimate spatially varying discharge fluxes. While small discharge fluxes (<43 m^3/s) feed numerous, deeply undercut outlets with subsurface plumes, ~70% of the net subglacial flux emerges at the terminus center, producing a vigorous, surface-reaching plume. This primary outlet drives large, localized seasonal retreat that exceeds calving rates at secondary outlets.

Plain Language Summary Using a sensor to map the shape of a glacier terminus below sea level, we are able to quantify how the terminus shape changes across the glacier. This allows us to identify different classes of terminus shape, which vary from undercut to overcut. Undercut regions are formed through melting focused near the base of the terminus, where freshwater emerges from discrete channels. Using a model, we explain the degree of undercutting found in channels by varying the flux of freshwater emerging from each channel. This allows us to understand the relative role of small channels on total terminus melt compared to much larger, more frequently observed channels. We find that small channels produce significant melting compared to a much larger channel at the glacier center but not as much iceberg calving.

1. Introduction

Frontal ablation (a combination of submarine melting and iceberg calving) at the termini of marine-terminating glaciers around the Greenland Ice Sheet may be increasing due to recent increases in surface meltwater production and ocean thermal forcing along the ice sheet periphery (Howat et al., 2008; Motyka et al., 2011; Straneo & Heimbach, 2013). This, in turn, has dramatic impacts on the dynamics of inland ice (Csatho et al., 2014; Enderlin et al., 2014; Felikson et al., 2017). Unfortunately, correctly simulating marine-terminating glacier retreat in ocean-ice models remains problematic. In part, this is because of unresolved small-scale processes that control the rates and spatial pattern of frontal ablation below the ocean surface (Straneo & Cenedese, 2015; Sutherland et al., 2019; Truffer & Motyka, 2016) and a lack of direct observations that prevent us from understanding how these processes impact the rate of terminus change. Indirect observations of terminus shape in map view indicate that calving is sensitive to the distribution of subglacial channel outlets, possibly as enhanced submarine melt undermines the integrity of the ice face in these regions (Benn et al., 2007; Chauché et al., 2014; Fried et al., 2015; Luckman et al., 2015). Direct observations of the submarine terminus provides a more complete understanding of terminus retreat.

Within the submarine environment, subglacial discharge (hereafter referred to as discharge) emerges at the grounding line, producing buoyant plumes that can increase frontal ablation (Motyka et al., 2003; Motyka et al., 2013; Rignot et al., 2010). While plume-driven melting can drive significant terminus retreat (Amundson & Carroll, 2018; Fried et al., 2018; Slater et al., 2018), numerical simulations of near-glacier circulation (Carroll et al., 2015; Kimura et al., 2014; Slater et al., 2015) rely on highly idealized characteristics of
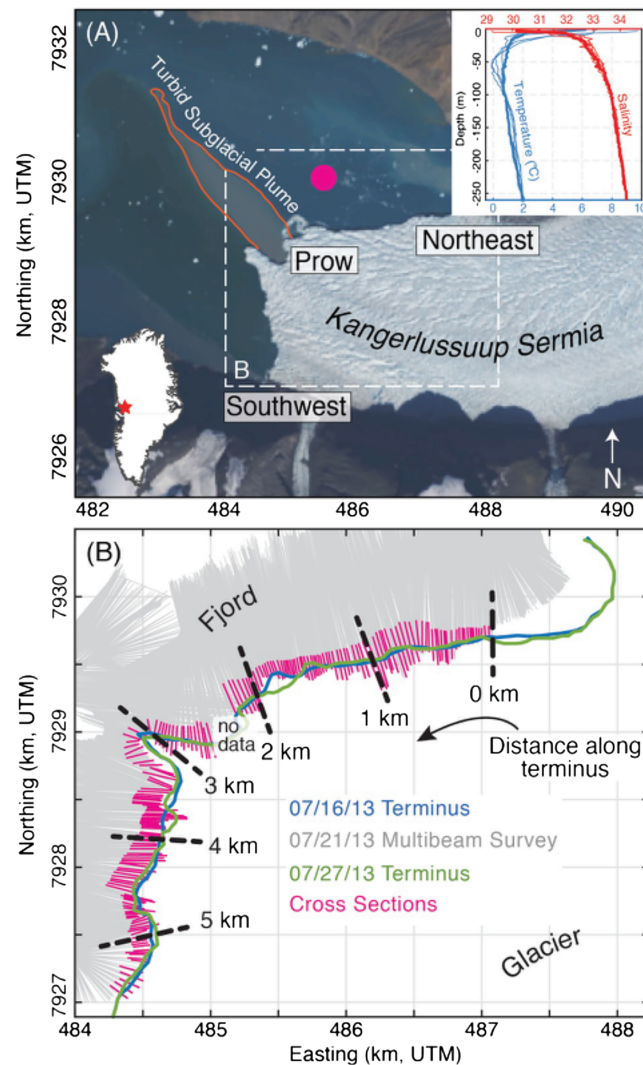
Figure 1. (a) Landsat image showing Kangerlussuup Sermia terminus. Temperature and salinity plot detailing fjord stratification is shown as an inset; thick lines represent the near-glacier profiles used for plume modeling (cast location shown as magenta circle). (b) Map showing locations of raw multibeam returns (gray); 190 terminus cross sections through the multibeam point cloud (magenta lines); map-view terminus positions on either side of the multibeam survey (16 July 2013 in blue and 27 July 2013 in green). Black dashed lines show distance markers along the segmented terminus (0 km in the northeast to ~5.5 km in the southwest).

discrete discharge outlets (hereafter referred to as outlets), such as spatial distribution, width, and depth. Furthermore, large uncertainties remain for estimates of outlet discharge in Greenland fjords, which have been constrained using fjord water properties (Chauché et al., 2014; Jackson et al., 2017; Stevens et al., 2016) and can strongly influence near-glacier circulation and melt rates (Carroll et al., 2015; Fried et al., 2015; Slater et al., 2018). In addition, ambient melting (outside of discharge outlets) may be an important source of terminus melt that is not well understood (Slater et al., 2018; Sutherland et al., 2019; Wagner et al., 2019). Ultimately, the connection between frontal ablation and terminus morphology is largely unknown, which limits our ability to parameterize the complete fjord-terminus-glacier system in coupled ocean-ice models.

In this paper, we present a detailed survey of submarine terminus morphology across Kangerlussuup Sermia (KAS), a tidewater glacier in central west Greenland (71°27′N, 51°20′W; Figure 1a). We identify and map distinct terminus morphologies and use these morphologies to infer the spatial distribution of frontal ablation processes acting across the ice face. We combine these observations with a buoyant plume model (Jackson et al., 2017; Jenkins, 2011) to estimate discharge fluxes, melt rates, and plume properties along the terminus.

2. Methods

KAS, is a well-grounded, tidewater glacier that is ~4.5 km wide and ~200 m deep and has remained stable for the last ~60 years (Catania et al., 2018). To map terminus morphology, we surveyed the KAS submarine lterminus using a multibeam sensor on 21 and 23 July 2013, which is accurate to within 3–5 m horizontally and 15–25 cm radially from the ship (described in Fried et al., 2015). Depths are referenced to mean sea level. We quantify changes in map-view terminus position at KAS using terminus positions from 16 and 27 July 2013 (Figure 1b) selected from 20-m resolution TerraSAR-X satellite imagery (courtesy of the German Aerospace Center, DLR) and available from Catania et al. (2018). These images bracket the timing of the submarine survey.

2.1. Quantifying Terminus Morphology

To quantify the shape of the submarine terminus, we aggregate the multibeam point cloud into 190 cross sections (mean spacing of 27 m), each oriented normal to the terminus face (Figure 1b). At each cross section, we extract all returns within 10 m of the cross section line and collapse these onto a 2-D cross section plane (Figure S1 in the supporting information), representing their distance along the terminus cross section and vertical depth (x coordinate and z coordinate, respectively). We do not quantify terminus shape across a ~200-m-wide segment at the center (hereafter referred to as the prow; Figure 1b), where the multibeam was unable to resolve the terminus face. The prow is deeply undercut and collocated with a turbid subglacial plume that consistently reaches the fjord surface during the melt season (Fried et al., 2015; Jackson et al., 2017); these factors likely obscured multibeam imaging. At each cross section, we remove seafloor bathymetry and anomalous multibeam returns (Figure S1); the seafloor boundary is determined using contrasts in slope between the horizontal seafloor and vertical terminus. We assume all returns along the terminus face represent glacier ice. Finally, to generate vertical terminus profiles we interpolate each cross section across the terminus (5-m horizontal and vertical resolution) and apply a 30-m running mean in the vertical to eliminate high-frequency noise.

From 190 terminus profiles, we compute the position and depth of the grounding line and seaward-most point (SMP) on the terminus face (Figure 2). The SMP represents the furthermost terminus position at each profile in the proglacial fjord. We estimate terminus slope (measured from the horizontal), as a function of depth at midpoints along 5-m intervals along each terminus profile (Figure 2). Using vertical profiles of terminus slope, we compute the mean, minimum, and maximum terminus slope at each profile location (Figure S2). Finally, we use the horizontal distance from the SMP and the point along the terminus profile that is furthest from the SMP (Figure 2) to compute the undercut length (if the SMP is above the furthest point) or the overcut length (if the SMP is below the furthest point). Undercut/overcut lengths can then be viewed across the entire terminus face with the distance above (overcut) or below (undercut) the local SMP (Figure 3a).

2.2. Modeling Discrete Subglacial Plumes

We model subglacial plumes at discrete outlets (identified as the laterally constricted terminus areas where undercutting exceeds 100 m) using buoyant plume theory (Jenkins, 2011) to constrain discharge fluxes required to reproduce observed channel outlets and resulting melt rates. Specifically, we use a truncated line plume geometry initialized with our observed outlet widths and depths; this model formulation has been shown to best fit in situ ocean observations at KAS (Jackson et al., 2017). We assume a vertical ice face, as modeled plume dynamics for near-vertical tidewater glaciers are independent of terminus slope (Slater et al., 2017). Using the plume model, we compute vertical profiles of plume velocity and melt rate along the ice face. We define the maximum plume height as the depth where the modeled plume velocity equals 0. Model fjord temperature and salinity are prescribed from a CTD cast collected <1 km from the KAS terminus on 21 July 2013 (Figure 1); this profile is consistent with previous summer KAS hydrographic observations (Carroll et al., 2018; Jackson et al., 2017).

3. Results

3.1. Ice Face Profiles

Multibeam point cloud data reveal significant heterogeneity in submarine terminus morphology (Figure 2) with four distinct submarine morphologies: (1) overcut, (2) undulating undercut, (3) gently undercut, and (4)
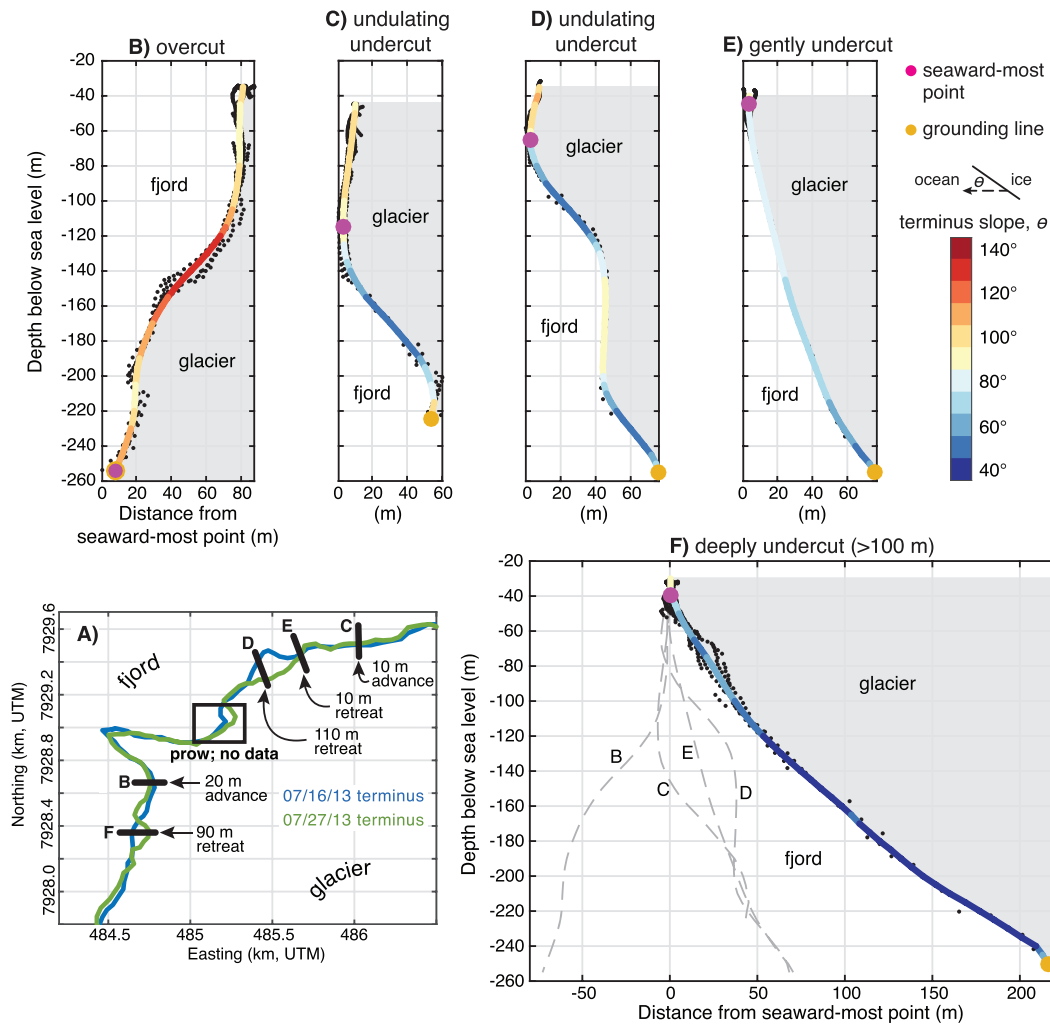
Figure 2. Characteristic terminus face profiles. (a) Map of cross section locations and corresponding terminus position change before (blue) and after (green) the multibeam survey. Panels (b)–(f) show observed terminus morphologies: (b) overcut, (c, d) undulating undercut, (e) gently undercut, and (f) deeply undercut. Gray dashed lines in (f) show terminus profiles from (b)–(e). Cross sections have equal length scales and aspect ratios. Terminus profiles are colored by terminus slope. The seaward-most point and grounding line are shown as magenta and yellow markers, respectively; black circles represent multibeam returns.

deeply undercut. Overcut profiles are characterized by SMPs located at the grounding line (Figures 2b and S3). Above the grounding line, the average terminus face slopes toward glacier more than 90° and, in some cases, exceeds 120°. Overcut lengths are generally <50 m but occasionally exceed 100 m. Additionally, all overcut profiles are texturally rough (on scales of tens of meters) and include middepth notches defined by abrupt changes in slope.

Undulating morphologies are characterized by SMPs located at intermediate depths. Here weak overcutting is found above undercut cavities (Figures 2c and 2d), with undercutting at the grounding line extending tens of meters behind the SMP and terminus slopes within these cavities limited to 50–60°. Maximum undercutting is found not only near the grounding line but also at intermediate depths in undulating profiles (Figure 2d). In some cases, the ice face protrudes into the proglacial fjord near the grounding line, forming glacial toes (labeled "g.l. toes" in Figure 3c). Undulating profiles exhibit large variability in terminus slope across the terminus (Figure S2).

Undercut morphologies are characterized as either gently or deeply undercut (Figures 2e and 2f). Gently undercut morphologies have smooth gradients in slope, maximum undercutting <100 m near the grounding line, and SMPs near the fjord surface. Gently undercut slopes are generally 60–90°, have a slope angle that
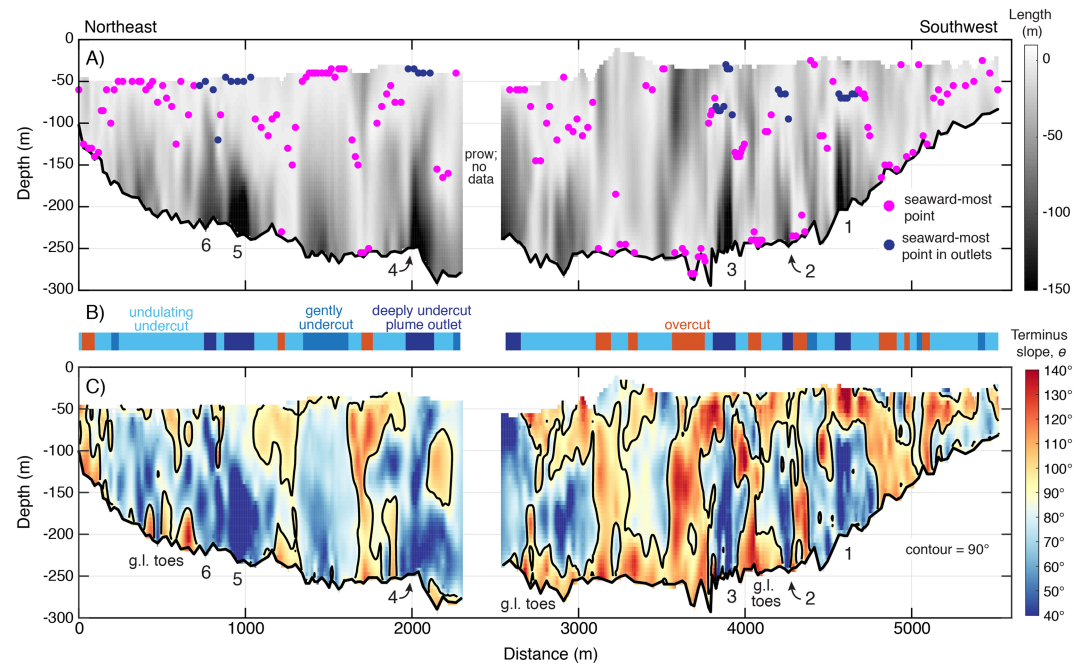
Figure 3. (a) Terminus regions and lengths calculated above (overcut) or below (undercut) the local seaward-most point (shown as magenta markers and blue markers within identified outlets). Identified outlets are labeled 1–6, and outlet 3 is shown as profile F in Figure 2. (b) Distribution of morphologies as identified in vertical terminus profiles. (c) Terminus slope, measured from the horizontal. Black contour represents 90°; grounding line toes are annotated.

decreases with depth, have the smallest interquartile range of slopes, and are morphologically smooth (Figures 2e and S2). Deeply undercut morphologies (Figures 2f and S4) represent extreme cases of gently undercut morphologies; we assume that these are the locations of subglacial channel outlets. They have maximum undercutting at the grounding line exceeding 100 m, shallow SMP depths (30–120 m), and smaller slopes than other morphologies (Figure S2). Six deeply undercut outlets, each less than 150 m wide, are identified in the KAS terminus (Figure 3 and Table 1).

3.2. Description of Mapped Terminus Morphology

The majority of the terminus face is undercut (77%), which includes both undulating, gently , and deeply undercut profiles (Figure 3). Roughly 40% of undulating regions exhibit small glacial toes that occur near the grounding line (Figure 3c). The six deeply undercut outlets comprise ~15% of the terminus face and are dispersed across the glacier front. Gently undercut morphologies are typically confined to a ~350-m-wide region along the northeast terminus (Figure 3, 1,300–1,650 m on *x* axis). The remaining 23% of the across-

Table 1
Outlet Characteristics and Estimated Discharge Fluxes From Plume Model

Outlet #	Outlet depth (m)	Outlet width (m)	Min/max SMP depth (m)	Mean SMP depth (m)	Modeled mean melt rate (m/day)	Model flux needed to match mean SMP depth (m³/s)	Model flux needed to shoal plume (m³/s)
1	−200	70	−65/−70	−69	1.23 ± 0.32	3.5 [2.5, 4.5]	87
2	−240	30	−65/−95	−80	1.48 ± 0.41	2 [1, 3]	47
3	−245	85	−30/−90	−63	1.78 ± 0.50	10 [7.5, 14]	130
4	−250	125	−35/−40	−39	2.49 ± 0.69	42.5 [33, 51]	185
5	−225	130	−45/−50	−49	1.97 ± 0.53	24.5 [19, 31.5]	166
6	−220	110	−50/−115	−80	1.29 ± 0.35	5.5 [4, 7.5]	121
Prow	−250	200	n/a	n/a	~3.1	200	200

Note. Values in column 6 represent mean ± two standard deviations. Bracketed values in column 7 represent the range of modeled flux needed to match the mean seaward-most point (SMP) depth given outlet geometry uncertainty (±10 and 15 m in outlet depth and width, respectively). Prow values are from Jackson et al. (2017).

face profiles are overcut, with the largest overcut region located near outlet 3 ($x = 3,700$ m in Figures 3a and 3b).

3.3. Constraints on Spatially Distributed Discharge Fluxes

Previous modeling work suggests that the vertical extent of undercutting may be controlled by the maximum plume rise height (Slater et al., 2017). Therefore, observed SMPs could act as a proxy for the vertical extent of plume-driven melting within outlets. Using our observations of deeply undercut morphologies at outlets (Table 1) and the plume model, we estimate discharge fluxes emerging from each outlet based on the assumption that undercutting is determined by the maximum plume height. We run the plume model with a range of discharge fluxes to constrain the flux that produces plumes with maximum rise heights equal to the observed SMPs (Table 1 and Figures S5 and S6). Although this approach depends on several assumptions, it acts as a conservative discharge estimate since the SMP is assumed to be the maximum possible plume height.

From the six identified outlets, modeled discharge fluxes range from 2–42.5 m^3/s, with a mean flux of 14.6 m^3/s and a total discharge flux of 88 m^3/s. Modeled mean melt rates within these outlets range between 1.25 and 2.5 m/day, with the highest melt rates associated with the largest discharge fluxes (Table 1). We find that given realistic bounds on the observed geometry, maximum plume heights correspond more directly to changes in discharge flux than outlet width and depth (Figure S6). In shallow, narrow outlets, plumes obtain their maximum height near the fjord surface, due to increased buoyancy fluxes per unit width and reduced entrainment of ocean waters. Substantially larger discharge fluxes are required for plumes to reach the fjord surface above SMPs (Table 1).

4. Discussion

Our results provide a quantitative description of submarine terminus morphology across a Greenland tidewater glacier. For KAS, we propose that deeply undercut terminus shapes result from plume-driven melt and overcut morphologies result from calving processes. This is because (1) overcut terminus shapes are texturally rough (Figure 2b) and have large (>120°) slopes, (2) plume-driven melting would undercut the terminus face and cause it to be near horizontal (i.e., shallowly sloped; Slater et al., 2017), and (3) if the overcut profile resulted from ambient melting (Carroll et al., 2016; Slater et al., 2018), this would require higher melt rates at shallower depths, which is contrary to the observation of warmer waters at depth (Figure 1). This interpretation is supported by satellite-derived terminus position records taken on 5 and 16 July 2013 showing terminus retreat of ~150 m (Fried et al., 2018), which occurs in a region of extensive overcutting. Depth dependence in ocean velocities could drive more variance in upper-layer horizontal circulation and increase submarine melt, thus contributing to the development of overcut morphologies. Because the terminus is fully grounded (Fried et al., 2015) and overcut segments are laterally confined (width <50% of local ice thickness), overcutting is unlikely from buoyancy-induced calving. Additionally, our observations show that small, shallow overcut notches proximal to the tidewater line occur across a range of terminus morphologies (Figures S3 and S4). These features may result from ambient melting driven by warm near-surface waters during summer (Carroll et al., 2018; Jackson et al., 2017), near-glacier secondary circulation (Carroll et al., 2017; Slater et al., 2018), or tidal forcing, which can trigger frequent, small-magnitude serac failure (Bartholomaus et al., 2015; How et al., 2019).

Previous studies show that terminus undercutting can initiate calving (Bartholomaus et al., 2013; Ma & Bassis, 2019; O'Leary & Christoffersen, 2013) by connecting undercut cavities with surface crevasses (Fried et al., 2015) and removing support from overlying ice (How et al., 2019; Luckman et al., 2015). We propose that this mechanism is in place for deeply undercut regions. Terminus position records, combined with the observed morphologies, provide support for this because we observe terminus retreat >90 m above deeply undercut morphologies with shallow SMPs (Figure 2a). In contrast, we find terminus advance, or minimal retreat, where undercutting is restricted to deeper depths or where the terminus is overcut. Submarine melt can also promote full-thickness calving (Benn et al., 2017; Ma & Bassis, 2019); however, we do not observe this at KAS, possibly because melt is focused within outlets and bridging stresses across these outlets provide support to the ice. Finally, we note that our observations are temporally limited and further work is needed to understand the evolution of the calving face through time.

While incomplete multibeam data restrict complete mapping of the prow, Jackson et al. (2017) used ocean observations to estimate a discharge flux of ~200 m^3/s during July 2014, although this estimate may include some regions outside of the prow. Assuming a similar discharge flux for KAS in July 2013 (e.g., Fried et al., 2018), we estimate that outlets are fed by a total of ~288 m^3/s during the peak melt season, with 70% of the discharge flux emerging from the prow. This is in good agreement with mean July 2013 runoff (~240 m^3/s) estimated from the RACMO2.3 model (Noël et al., 2016) based on daily runoff values integrated over the glacier catchment (Fried et al., 2018). While the KAS terminus is stable, it does experience seasonal fluctuations in position, with the majority of seasonal terminus change concentrated at the prow (Fried et al., 2018). This is also where the largest outlet exists and a persistent turbid plume is visible on the fjord surface (Figure 1); thus, we argue that calving is enhanced in this region due to severe undercutting, similar to How et al. (2019). We further speculate that ~70% of the total discharge delivered to the terminus, the percentage of our budget estimated by Jackson et al. (2017) at the prow, controls the majority of terminus position change over the melt season.

SMPs in outlets are often clustered proximal to the near-surface pycnocline at 60–80 m (e.g., outlets 1–3 in Figure 3), suggesting potential feedbacks between fjord stratification, plume height, and terminus morphology. In Greenland fjords, stratification typically consists of three layers: salty Atlantic-origin waters at depth (~150–200 m); cold, fresh Polar-origin waters at intermediate depths (~50–200 m); and a warm seasonal layer of surface water (<50 m; Carroll et al., 2016; Straneo et al., 2012; e.g., Figure 1). Previous observational (Straneo et al., 2011) and modeling efforts (Carroll et al., 2015; Sciascia et al., 2013) have shown that outflowing plume waters are often concentrated near the density interface between Polar- and Atlantic-origin waters and the near-surface pycnocline. This suggests that fjord stratification may act, in part, to delineate undercut and overcut terminus morphologies by regulating maximum plume height.

Additionally, modeled maximum plume heights are more sensitive to discharge flux than outlet width and depth, given the range of observed outlet geometries (Figure S6). The discharge flux required for plumes to penetrate through the pycnocline and reach the fjord surface is unrealistic for small, deep outlets (Table 1), since the cumulative discharge across the terminus would drastically exceed RACMO runoff estimates. Additionally, we do not observe surface-reaching plumes at these secondary outlets in the satellite record (Fried et al., 2015). Overall, these observations suggest that smaller subglacial plumes drive substantial submarine melting and undercutting at depth but may be insufficient to trigger large-scale calving that controls seasonal terminus retreat.

Our results provide constraints for modeling subglacial plume dynamics across tidewater glacier termini. First, in order to compute net submarine melt and prescribe the flux of glacially modified waters in fjord/coastal grid cells, future modeling should not neglect the role of secondary outlets (Slater et al., 2015). While these outlets are generally fed by small fluxes (<50 m^3/s), they can have a significant influence on net terminus melt (Fried et al., 2015), fjord-scale circulation (Carroll et al., 2015), and the properties of outflowing glacially modified waters (Beaird et al., 2018; Carroll et al., 2017). We note that plume properties, and hence the ocean waters in contact with the terminus face, may be drastically different between primary and secondary outlets, as plume temperature and salinity are strongly dependent on discharge flux and outlet geometry (Carroll et al., 2016, 2017; Slater et al., 2016). This implies that the role of plume entrainment in secondary outlets, which can result in strongly diluted subsurface plumes (Carroll et al., 2015), should be explicitly accounted for. For estimates of melt-driven calving, we suggest that a focus primarily on the largest outlets may be sufficient. For shallowly grounded glaciers (<300 m), plumes are most likely to drive substantial undercutting, which can reach surface crevasses. Together, these observations provide implications for the role of subglacial discharge and plumes in driving melt (e.g.Benn et al., 2017, Motyka et al., 2013, Slater et al., 2018), calving (e.g.Luckman et al., 2015, O'Leary & Christoffersen, 2013), and fjord properties (e.g.Carroll et al., 2017, Sciascia et al., 2013) for tidewater glaciers.

5. Summary and Conclusions

To better constrain the mechanisms that control frontal ablation, we present direct observations of terminus morphology at a glacier in central West Greenland. We characterize distinct terminus morphologies that are indicative of calving and submarine melting processes: (1) overcut, (2) undulating undercut, (3) gently undercut, and (4) deeply undercut. The majority of the terminus (~77%) is undercut, likely driven by

submarine melting at depth. In contrast, full-thickness overcut regions are likely driven by calving and comprise ~23% of the terminus.

Our results provide constraints on the geometry and location of six deeply undercut discharge outlets that occur outside of the primary outlet. Relatively small discharge fluxes within these secondary outlets are required to generate modeled plume rise heights that agree with the observed outlet geometries. For the observed stratification and range of terminus geometries, plume rise heights are more sensitive to changes in discharge flux than variability in outlet geometry. Unrealistically large discharge fluxes are required to produce plumes that penetrate through the near-surface pycnocline; as a result, plume-driven undercutting is primarily confined to depth. While these secondary outlets produce substantial undercutting when integrated across the terminus, seasonal terminus change is largest at the terminus center, where the majority of subglacial discharge (~70%) drives a persistent, surface-reaching plume. Ultimately, these observations provide constraints on the submarine terminus environment and can be used to inform parameterizations of frontal ablation processes.

References

Amundson, J. M., & Carroll, D. (2018). Effect of topography on subglacial discharge and submarine melting during tidewater glacier retreat. *Journal of Geophysical Research: Earth Surface*, *123*, 66–79. https://doi.org/10.1002/2017JF004376

Bartholomaus, T. C., Larsen, C., & O'Neel, S. (2013). Does calving matter? Evidence for significant submarine melt. *Earth and Planetary Science Letters*, *380*, 21–30.

Bartholomaus, T. C., Larsen, C. F., West, M. E., O'Neel, S., Pettit, E. C., & Truffer, M. (2015). Tidal and seasonal variations in calving flux observed with passive seismology. *Journal of Geophysical Research: Earth Surface*, *120*, 2318–2337. https://doi.org/10.1002/2015JF003641

Beaird, N. L., Straneo, F., & Jenkins, W. (2018). Export of strongly diluted Greenland meltwater from a major glacial fjord. *Geophysical Research Letters*, *45*, 4163–4170. https://doi.org/10.1029/2018GL077000

Benn, D. I., Åström, J., Zwinger, T., Todd, J., Nick, F., Cook, S., et al. (2017). Melt-under-cutting and buoyancy-driven calving from tidewater glaciers: New insights from discrete element and continuum model simulations. *Journal of Glaciology*, *63*(240), 691–702.

Benn, D. I., Warren, C. R., & Mottram, R. H. (2007). Calving processes and the dynamics of calving glaciers. *Earth-Science Reviews*, *82*, 143–179.

Carroll, D., Sutherland, D. A., Curry, B., Nash, J. D., Shroyer, E. L., Catania, G. A., et al. (2018). Subannual and seasonal variability of Atlantic-origin waters in two adjacent west Greenland fjords. *Journal of Geophysical Research: Oceans*, *123*, 6670–6687. https://doi.org/10.1029/2018JC014278

Carroll, D., Sutherland, D. A., Hudson, B., Moon, T., Catania, G. A., Shroyer, E. L., et al. (2016). The impact of glacier geometry on meltwater plume structure and submarine melt in Greenland fjords. *Geophysical Research Letters*, *43*, 9739–9748. https://doi.org/10.1002/2016GL070170

Carroll, D., Sutherland, D. A., Shroyer, E. L., Nash, J. D., Catania, G., & Stearns, L. A. (2015). Modeling turbulent subglacial meltwater plumes: Implications for fjord-scale buoyancy-driven circulation. *Journal of Physical Oceanography*, *45*, 2169–2185.

Carroll, D., Sutherland, D. A., Shroyer, E. L., Nash, J. D., Catania, G. A., & Stearns, L. A. (2017). Subglacial discharge-driven renewal of tidewater glacier fjords. *Journal of Geophysical Research: Oceans*, *122*, 6611–6629. https://doi.org/10.1002/2017JC012962

Catania, G. A., Stearns, L. A., Sutherland, D. A., Fried, M. J., Bartholomaus, T. C., Morlighem, M., et al. (2018). Geometric controls on tidewater glacier retreat in central Western Greenland. *Journal of Geophysical Research: Earth Surface*, *29*, 1–15. https://doi.org/10.1029/2017JF004499

Chauché, N., Hubbard, A., Gascard, J. C., Box, J. E., Bates, R., Koppes, M., et al. (2014). Ice–ocean interaction and calving front morphology at two west Greenland tidewater outlet glaciers. *The Cryosphere*, *8*, 1457–1468.

Csatho, B. M., Schenk, A. F., van der Veen, C. J., Babonis, G., Duncan, K., Rezvanbehnahani, S., et al. (2014). Laser altimetry reveals complex pattern of Greenland ice sheet dynamics. *Proceedings of the National Academy of Sciences of the United States of America*, *111*(52), 18,478–18,483.

Enderlin, E. M., Howat, I. M., Jeong, S., Noh, M. J., Angelen, J. H., & Broeke, M. R. (2014). An improved mass budget for the Greenland ice sheet. *Geophysical Research Letters*, *41*, 866–872. https://doi.org/10.1002/2013GL059010

Felikson, D., Bartholomaus, T. C., Catania, G. A., Korsgaard, N. J., Kjaer, K. H., Morlighem, M., et al. (2017). Inland thinning on the Greenland Ice Sheet controlled by outlet glacier geometry. *Nature Geoscience*, *10*, 366–369.

Fried, M. J., Catania, G. A., Bartholomaus, T. C., Duncan, D., Davis, M., Stearns, L. A., et al. (2015). Distributed subglacial discharge drives significant submarine melt at a Greenland tidewater glacier. *Geophysical Research Letters*, *42*, 9328–9336. https://doi.org/10.1002/2015GL065806

Fried, M. J., Catania, G. A., Stearns, L. A., Sutherland, D. A., Bartholomaus, T. C., Shroyer, E. L., & Nash, J. D. (2018). Reconciling drivers of seasonal terminus advance and retreat at thirteen central west Greenland tidewater glaciers. *Journal of Geophysical Research: Earth Surface*, *123*, 1590–1607. https://doi.org/10.1029/2018JF004628

How, P., Schild, K., Benn, D., Noormets, R., Kirchner, N., Luckman, A., et al. (2019). Calving controlled by melt-under-cutting: Detailed calving styles revealed through time-lapse observations. *Annals of Glaciology*, *60*(78), 20–31.

Howat, I., Joughin, I., Fahnestock, M., Smith, B., & Scambos, T. A. (2008). Synchronous retreat and acceleration of southeast Greenland outlet glaciers 2000-06: Ice dynamics and coupling to climate. *Journal of Glaciology*, *54*(187), 646–660.

Jackson, R. H., Shroyer, E. L., Nash, J. D., Sutherland, D. A., Carroll, D., Fried, M. J., et al. (2017). Near-glacier surveying of a subglacial discharge plume: Implications for plume parameterizations. *Geophysical Research Letters*, *44*, 6886–6894. https://doi.org/10.1002/2017GL073602

Jenkins, A. (2011). Convection-driven melting near the grounding lines of ice shelves and tidewater glaciers. *Journal of Physical Oceanography*, *41*, 2279–2294.

Kimura, S., Holland, P. R., Jenkins, A., & Piggott, M. (2014). The effect of meltwater plumes on the melting of a vertical glacier face. *Journal of Physical Oceanography*, *44*, 3099–3117.

Luckman, A., Benn, D. I., Cottier, F., Bevan, S., Nilsen, F., & Inall, M. (2015). Calving rates at tidewater glaciers vary strongly with ocean temperature. *Nature Communications*, *6*, 8566.

Ma, Y., & Bassis, J. N. (2019). The effect of submarine melting on calving from marine terminating glaciers. *Journal of Geophysical Research: Earth Surface*, *124*, 334–346. https://doi.org/10.1029/2018JF004820

Motyka, R., Dryer, W. P., Amundson, J., Truffer, M., & Fahnestock, M. (2013). Rapid submarine melting driven by subglacial driven by subglacial discharge, LeConte Glacier, Alaska. *Geophysical Research Letters*, *40*, 5153–5158. https://doi.org/10.1002/grl.51011

Motyka, R., Hunter, L., Echelmeyer, K., & Connor, C. (2003). Submarine melting at the terminus of a temperate tidewater glacier, LeConte Glacier, Alaska, U.S.A. *Annals of Glaciology*, *36*, 57–65.

Motyka, R. J., Truffer, M., Fahnestock, M., Mortensen, J., Rysgaard, S., & Howat, I. (2011). Submarine melting of the 1985 Jakobshavn Isbræ floating tongue and the triggering of the current retreat. *Journal of Geophysical Research*, *116*, F01007. https://doi.org/10.1029/2009JF001632

Noël, B., Jan van de Berg, W., Machguth, H., Lhermitte, S., Howat, I., Fettweis, X., & van den Broeke, M. R. (2016). A daily, 1 km resolution data set of downscaled Greenland ice sheet surface mass balance (1958–2015). *The Cryosphere*, *10*, 2361–2377.

O'Leary, M., & Christoffersen, P. (2013). Calving on tidewater glaciers amplified by submarine frontal melting. *The Cryosphere*, *7*, 119–128.

Rignot, E., Koppes, M., & Velicogna, I. (2010). Rapid submarine melting of the calving faces of west Greenland glaciers. *Nature Geoscience*, *3*, 187–191.

Sciascia, R., Straneo, F., Cenedese, C., & Heimbach, P. (2013). Seasonal variability of submarine melt rate and circulation in an East Greenland fjord. *Journal of Geophysical Research: Oceans*, *118*, 2492–2506. https://doi.org/10.1002/jgrc.20142

Slater, D., Straneo, F., Das, S., Richards, C., Wagner, T., & Nienow, P. (2018). Localized plumes drive front-wide ocean melting of a Greenlandic tidewater glacier. *Geophysical Research Letters*, *45*, 12,350–12,358. https://doi.org/10.1029/2018GL080763

Slater, D. A., Goldberg, D. N., Nienow, P. W., & Cowton, T. R. (2016). Scalings for submarine melting at tidewater glaciers from buoyant plume theory. *Journal of Physical Oceanography*, *46*, 1839–1855.

Slater, D. A., Nienow, P. W., Cowton, T. R., Goldberg, D. N., & Sole, A. J. (2015). Effect of near-terminus subglacial hydrology on tidewater glacier submarine melt rates. *Geophysical Research Letters*, *42*, 2861–2868. https://doi.org/10.1002/2014GL062494

Slater, D. A., Nienow, P. W., Goldberg, D. N., Cowton, T. R., & Sole, A. J. (2017). A model for tidewater glacier undercutting by submarine melt. *Geophysical Research Letters*, *44*, 2360–2368. https://doi.org/10.1002/2016GL072374

Stevens, L. A., Straneo, F., Das, S. B., Plueddemann, A. J., Kukulya, A. L., & Morlighem, M. (2016). Linking glacially modified waters to catchment-scale subglacial discharge using autonomous underwater vehicle observations. *The Cryosphere*, *10*, 417–432.

Straneo, F., & Cenedese, C. (2015). The dynamics of Greenland's glacial fjords and their role in climate. *Annual Review of Marine Science*, *7*(1), 89–112.

Straneo, F., Curry, R., Sutherland, D., Hamilton, G., Cenedese, C., Vage, K., & Stearns, L. (2011). Impact of fjord dynamics and glacial runoff on the circulation near Helheim Glacier. *Nature Geoscience*, *4*(5), 322–327.

Straneo, F., & Heimbach, P. (2013). North Atlantic warming and the retreat of Greenland's outlet glaciers. *Nature*, *504*, 36–43.

Straneo, F., Sutherland, D., Holland, D., Gladish, C., Hamilton, G., Johnson, H., et al. (2012). Characteristics of ocean waters reaching Greenland's glaciers. *Annals of Glaciology*, *53*(60), 202–210.

Sutherland, D. A., Jackson, R. H., Kienholz, C., Amundson, J. M., Dryer, W. P., Duncan, D., et al. (2019). Direct observations of submarine melt and subsurface geometry at a tidewater glacier. *Science*, *365*(6451), 369–374.

Truffer, M., & Motyka, R. (2016). Where glaciers meet water: Subaqueous melt and its relevance to glaciers in various settings. *Reviews of Geophysics*, *54*, 220–239. https://doi.org/10.1002/2015RG000494

Wagner, T. J. W., Straneo, F., Richards, C. G., Slater, D. A., Stevens, L. A., Das, S. B., & Singh, H. (2019). Large spatial variations in the flux balance along the front of a Greenland tidewater glacier. *The Cryosphere*, *13*, 911–925.